Nanoscale

COMMUNICATION

View Article Online
View Journal | View Issue

Cite this: *Nanoscale*, 2015, **7**, 8689

Received 13th January 2015,
Accepted 15th April 2015

DOI: 10.1039/c5nr00251f

www.rsc.org/nanoscale

Payload drug *vs*. nanocarrier biodegradation by myeloperoxidase- and peroxynitrite-mediated oxidations: pharmacokinetic implications†

Wanji Seo,[a] Alexandr A. Kapralov,[b] Galina V. Shurin,[c] Michael R. Shurin,[c,d] Valerian E. Kagan[b] and Alexander Star*[a]

With the advancement of nanocarriers for drug delivery into biomedical practice, assessments of drug susceptibility to oxidative degradation by enzymatic mechanisms of inflammatory cells become important. Here, we investigate oxidative degradation of a carbon nanotube-based drug carrier loaded with Doxorubicin. We employed myeloperoxidase-catalysed and peroxynitrite-mediated oxidative conditions to mimic the respiratory burst of neutrophils and macrophages, respectively. In addition, we revealed that the cytostatic and cytotoxic effects of free Doxorubicin, but not nanotube-carried drug, on melanoma and lung carcinoma cell lines were abolished in the presence of tumor-activated myeloid regulatory cells that create unique myeloperoxidase- and peroxynitrite-induced oxidative conditions. Both *ex vivo* and *in vitro* studies demonstrate that the nanocarrier protects the drug against oxidative biodegradation.

Recent advances in the development of nanomaterials have provided a great opportunity for precise engineering in drug delivery.[1] Carbon nanotubes are particularly useful for intracellular drug delivery[2,3] and prolonged circulation times due to the enhanced permeability and retention (EPR) effect.[4] However, the inherent hydrophobicity of nanotubes necessitates surface modifications and functionalization with hydrophilic auxiliary components, and thus prediction of the long-term safety is even more complicated. Recent demonstration of peroxidase-mediated degradation of oxidized carbon nanotubes[5–7] has increased their potential significance in biomedical applications. The use of degradable drug carriers is imperative in clinical applications,[8] but their degradation may reduce drug efficacy and cause side effects—regardless of whether the degradation is programmed or naturally occurs.[9] It has been well documented that oxidative enzymes of inflammatory cells—upon their release into circulation—markedly accelerate oxidative biodegradation of numerous classes of drugs, thus affecting their therapeutic potential.[10–12] These studies, to the best of our knowledge, have not been conducted with nano-delivery drug formulations. Because oxidation mechanisms and degradation kinetics are highly dependent on the functional groups and surface properties of nanotubes as well as interactions with various endogenous oxidants,[13] the degradation characteristics of drug carriers should be thoroughly studied in the process of developing a new paradigm for carbon nanotube-based drug delivery.

This paper investigates the lifespan of the drug and the degradation behaviour of the single-walled carbon nanotube (SWCNT)-based drug carrier upon exposure to oxidative conditions mimicking oxidative burst of phagocytes, such as neutrophils (polymorphonuclear phagocytes) and monocytes/macrophages that are important components of white blood cells and different tissues. Here, we employ Doxorubicin (DOX) as a prototypical payload for a model drug delivery system (DOX-SWCNT), which constitutes an oxidized single-walled nanotube (ox-SWCNT) and a branched phospholipid-polyethylene glycol (PL-PEG) that has demonstrated excellent *in vivo* clearance and circulation times.[14–18] When drug nanocarriers are administered, the innate immune system recognizes them as a foreign substance and pathogens,[19–21] which can elicit unwanted immune responses to the drug.[22] Thus, understanding the oxidative metabolism of DOX-SWCNT will provide insights into designing smart drug delivery systems that impart with maximum drug resistance towards the innate immune system prior to the timely degradation of nanocarriers. Our study aims at investigating the oxidation of DOX-SWCNT under the oxidative burst. For oxidative conditions, we chose (1) myeloperoxidase and hydrogen peroxide in the presence of chloride ($MPO/H_2O_2/Cl^-$) and (2) peroxynitrite ($ONOO^-$), which neutrophils and macrophages

[a]*Department of Chemistry, University of Pittsburgh, Pittsburgh, PA 15260, USA. E-mail: astar@pitt.edu*
[b]*Department of Environmental and Occupational Health, University of Pittsburgh, 100 Technology Drive, Pittsburgh, PA 15219, USA*
[c]*Department of Pathology, University of Pittsburgh Medical Center, Pittsburgh, PA 15261, USA*
[d]*Department of Immunology, University of Pittsburgh Medical Center, Pittsburgh, PA 15261, USA*

† Electronic supplementary information (ESI) available: Experimental details and data from characterization of materials synthesis and degradation studies. See DOI: 10.1039/c5nr00251f

spontaneously release to intra- and extracellular domains during the host-immune response, particularly phagocytosis.[23,24] The MPO highly expressed in neutrophils catalyses the oxidation of chloride (Cl^-) with endogenous hydrogen peroxide (H_2O_2), which is further converted to hypochlorite/hypochlorous acid ($^-OCl/HOCl$) at physiological conditions.[25,26] Macrophages produce peroxynitrite ($ONOO^-$), which is formed in a reaction of nitric oxide ($^{\bullet}NO$) with superoxide ($O_2^{\bullet-}$).[24] The substances derived from the immune mechanism participate in antitumor as well as antimicrobial/anti-inflammatory activities.[27,28] While large numbers of neutrophils and macrophages are localized in the tumor microenvironment, the therapeutic effects of drugs in the vicinity of these areas may be significantly reduced due to increased oxidative activities by the strong oxidants.[29–31] Our group and others demonstrated that these strong oxidants are responsible for degrading carbon nanotubes,[5,6,32–34] and that oxidized carbon nanotubes were more susceptible to the biodegradation than pristine ones (non-functionalized nanotubes).[35,36] In spite of the promising results, the structural change of drug carriers may cause the untimely clearance of drug molecules. Also, DOX bound to the nanotube carrier may simultaneously undergo degradation on its own under the same oxidative conditions, thereby dramatically altering their original pharmacokinetic properties.

Here, we have studied the degradation kinetics of DOX-SWCNT in comparison with that of free DOX, and have demonstrated that the degradation rates of the drug molecules differed. Upon exposure to either $MPO/H_2O_2/Cl^-$ or peroxynitrite ($ONOO^-$), the drug molecules bound to the nanotube carrier exhibit slower oxidation rates than free DOX. On the other hand, non-oxidative conditions show pH-dependent degradation in which the degradation rates of DOX-SWCNT and free DOX are very similar.

DOX-SWCNT was synthesized following a published procedure.[14,15] Pristine HiPco SWCNTs were oxidized using a mixture of concentrated H_2SO_4/HNO_3 (3 : 1, v/v), yielding short oxidized nanotubes. PL-PEG (average MW *ca.* 7.4–8.2 KDa, Fig. S1†) was synthesized by coupling a branched PEG with a phospholipid-tethered PEG (Fig. 1a). The ox-SWCNTs were non-covalently functionalized with PL-PEG prior to non-covalent conjugation with DOX. The degree of oxidation of pristine HiPco SWCNT was measured by Raman spectroscopy, Fourier transform infrared spectroscopy (FTIR), and X-ray photoelectron spectroscopy (XPS) (Fig. S2–S4†). Fig. 1b–d show the transmission electron microscopy (TEM) images of each step of functionalization in the synthesis of DOX-SWCNT. Although most of the drug conjugate particles shown in Fig. 1d maintain high aspect ratios with an average length of 135 nm, agglomerates are relatively abundant.

UV-Vis-NIR absorption spectra confirm the presence of each component of the drug conjugate (Fig. 1e). The suppressed S_{11} optical transitions near 870–1100 nm are characteristic of oxidized HiPco SWCNTs,[37] in which the broad absorption band constitutes the residual peaks of numerous chiral species.[38] A slightly red-shifted DOX absorption maximum at 495 nm from the free DOX absorption (480 nm)

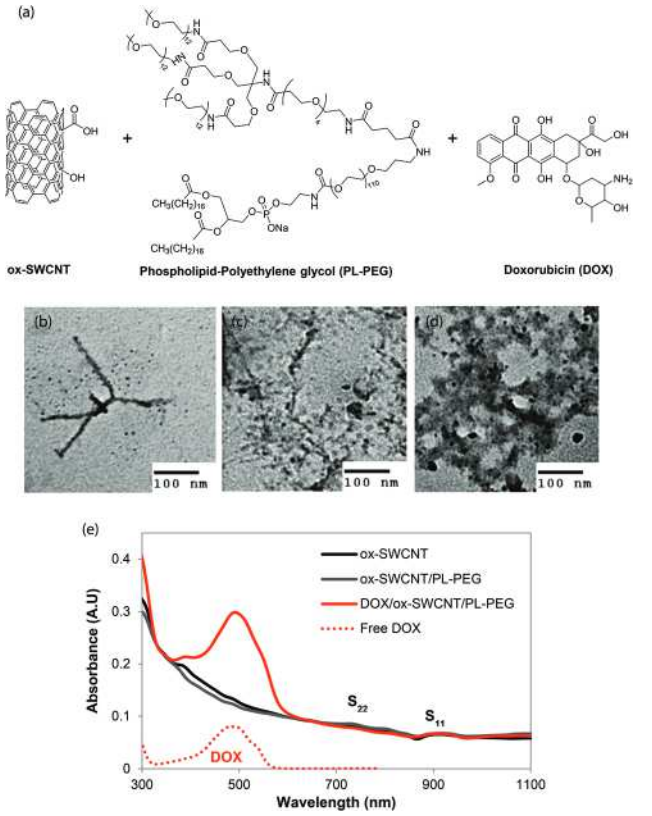

Fig. 1 (a) Chemical structures of the individual components, (b)–(d) TEM images of (b) oxidized HiPco (ox-SWCNT), (c) after functionalization with PL-PEG (ox-SWCNT/PL-PEG), and (d) loading with DOX/ox-SWCNT/PL-PEG (DOX-SWCNT). (e) UV-Vis-NIR absorption spectra for each functional nanomaterial. The spectra for SWCNT samples were normalized at 364 nm for comparison.

is indicative of non-covalent adsorption of drug molecules on the surface of ox-SWCNT,[39] which was further demonstrated by the quenched fluorescence emission of DOX *via* mainly π–π stacking[40] at 555 and 595 nm (Fig. S5†). The drug loading of DOX was measured by titrations using UV-Vis absorption spectroscopy (Fig. S6†) and zeta potential analysis under pH 7.0 (Fig. S7†). A binding ratio of DOX to the nanocarrier (weight of bound DOX/weight of ox-SWCNT/PL-PEG) was found to be approximately 1 : 1.

Next, we investigated the degradation profiles of the nanotube and DOX in phosphate buffer solution (0.1 M, pH 7.4) by monitoring spectral changes in UV-Vis-NIR absorption spectroscopy. Each sample contained NaCl (0.14 M) as a chloride source and diethylenetriaminepentaacetic acid (DTPA) as a chelating agent coordinating with residual transition metal catalyst ions present in the commercial HiPco nanotubes. The peroxidase-catalysed oxidation cycle was initiated by addition of an aliquot of H_2O_2 to MPO, which produced hypochlorous acid/hypochlorite ($HOCl/OCl^-$) equilibrating at pH 7.4 and reactive intermediate species (Fig. 2a).[5,32] Hypochlorite (OCl^-) can further induce oxidation, and MPO-I and MPO-II, each of which drives one-electron oxidation,[41] promote the form-

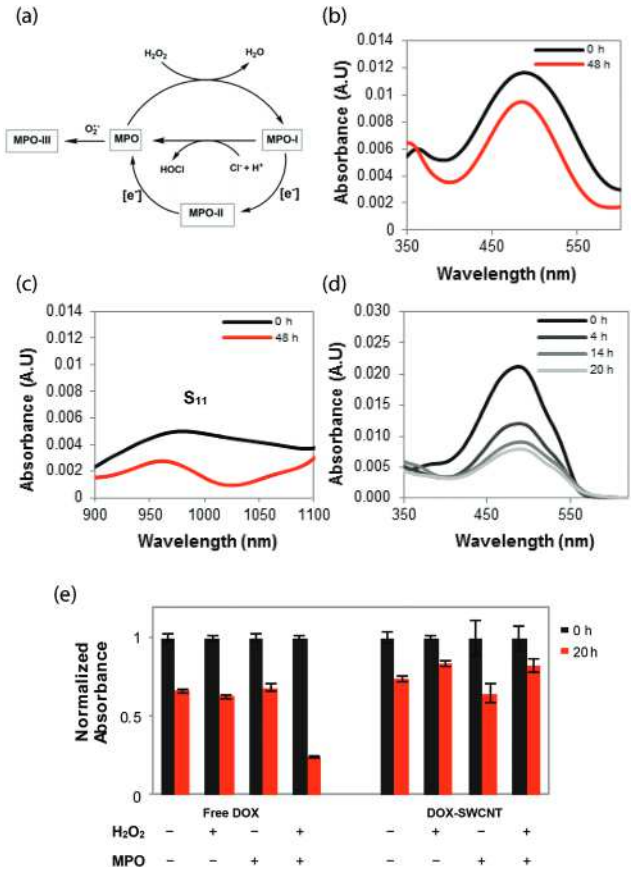

Fig. 2 MPO-catalysed oxidative degradation under pH 7.4 at 37 °C. (a) MPO catalytic cycle activated by H_2O_2 and production of HOCl. (b) Change in DOX absorbance (495 nm) and (c) S_{11} band (900–1100 nm) before and after 48 h. (d) Decreasing absorbance of free DOX over 20 h. (e) Degradation of DOX (free DOX *vs.* DOX-SWCNT) under four different conditions of (±) MPO/(±) H_2O_2. The error bars indicate the means ± SD of three replicate measurements.

ation of reactive radical intermediates and electron transfer reactions.

The samples were incubated at 37 °C, and the resulting spectral changes were recorded periodically at room temperature. In the presence of MPO/H_2O_2/Cl^-, Fig. 2b and c show decreases in absorbance of DOX at 495 nm and the S_{11} region (900–1100 nm) of ox-SWCNT. The absorption profile of the residual peaks near 950 nm changed significantly. Likewise, the NIR absorbance of ox-SWCNT/PL-PEG (no drug) decreased, indicating that the nanotube surface coated with the PL-PEG had also undergone oxidative degradation, as demonstrated by TEM (Fig. S8†). This result is in good agreement with previous degradation studies of PEG-SWCNTs that were non-covalently functionalized with PEGs of various molecular weights (*ca.* 600–10 000 Da).[42,43]

The dramatically different NIR absorption profiles over the course of degradation (Fig. 2c) suggest that the altered energy band gaps of the nanotubes possibly resulted from changes in the electronic structures and functional groups of the nanotube sidewall and ends. The oxidation of the drug carrier may

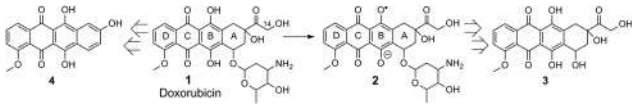

Scheme 1 MPO-catalysed and pH-dependent degradation of DOX at pH 7.4.

disrupt the π–π stacking of DOX and initiate dissociations of the drug molecules from the nanotube surface. This observation further raises a concern that the drug molecules could be untimely released during circulation. However, the relatively small change in the DOX absorption at 495 nm (Fig. 2b) compared to free DOX (Fig. 2d) indicates that most drug molecules still remained intact during the oxidation process. In the presence of MPO/H_2O_2/Cl^-, free DOX degraded about fourfold faster than DOX of the drug conjugate (Fig. 2e), which suggests that the nanotube carrier may serve as a scavenger for the strong oxidant ($^-$OCl) and reactive intermediate species generated from the MPO cycle. Because phenolic derivatives are especially good reducing substrates for the conversion of MPO-I into MPO-II,[44] ox-SWCNT carrier containing hydroxyl groups (Fig. S4b and c†) can facilitate competing reactions with DOX. We propose the major chemical transformations of DOX in Scheme 1, where **1** is likely to undergo radical reactions due to the hydroquinone (B-ring) adjacent to the electrophilic quinone (C-ring) moieties. The one-electron oxidation generates **2** (semiquinone ($O^{\bullet -}$) of B-ring), and **3** can be formed through multiple steps by electron transfer and radical rearrangement on the carbons of A- and B-ring in the presence of excess H_2O or $^-$OH.[45] Further proposed degradation products and competing reactions are discussed in ESI (Scheme S1†).

Interestingly, except for the free DOX under the MPO-catalysed oxidation, the drug molecules in all other samples degraded relatively evenly, considering that the error bars slightly overlap with one another (Fig. 2e). These similar degradation patterns in the non-enzymatic oxidative conditions for both free DOX and DOX-SWCNT samples indicate that DOX is somewhat unstable in the pH 7.4 buffer at 37 °C. We attributed this result to pH-dependent degradation resulting from keto–enol tautomerization upon deprotonation at C14 of **1**, followed by deacetylation and deglycosylation.[46] Our analyses with ^{1}H NMR and LC/MS confirmed the formation of **4** (Fig. S9–S11†).

In the analysis of peroxynitrite-mediated oxidation, we utilized fluorescence emission spectroscopy to investigate the stability of DOX-SWCNT because the absorption band of the by-product overlapped with that of free DOX (Fig. S12†). The drug conjugate was incubated in phosphate buffer (0.1 M, pH 7.4) at 37 °C. Peroxynitrite ($ONOO^-$) was generated *in situ* by the reaction of superoxide radicals ($O_2^{\bullet -}$) with nitric oxide ($^{\bullet}$NO) (Fig. 3a), where xanthine oxidase (xo) catalyses the oxidation of xanthine and produces superoxide radicals; and 3-(2-hydroxy-2-nitroso-1-propylhydrazino)-1-propanamine (PAPA NONOate) serves as a nitric oxide donor.

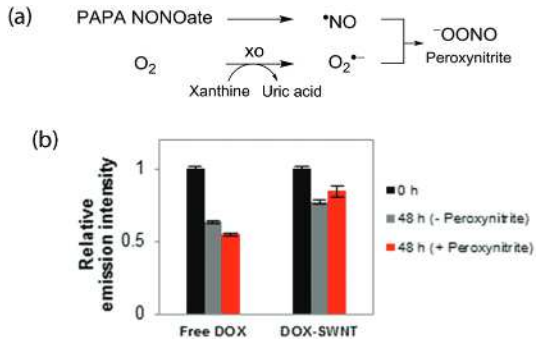

Fig. 3 (a) Formation of peroxynitrite (b) peroxynitrite-mediated degradation of free DOX *vs.* DOX-SWCNT in phosphate buffer (0.1 M, pH 7.4) at 37 °C. The error bars indicate the means ± SD of three replicate measurements.

As in the MPO-catalysed oxidation, the drug conjugate (DOX-SWCNT) shows a smaller change of DOX emission intensity than that of free DOX (Fig. 3b). It appears that the nanocarrier protects the drug molecules from the strong oxidant peroxynitrite ($ONOO^-$). The NIR band profiles and the TEM images of degrading ox-SWCNT/PL-PEG listed in ESI (Fig. S12 and S13†) demonstrate that the nanocarrier was subject to structural transformation, where peroxynitrite ($ONOO^-$) can promote (1) direct nucleophilic reactions and (2) one- or two-electron transfer oxidations.[32]

Peroxynitrite randomly diffuses through biological compartments and directly oxidizes SWCNTs. Similarly, HOCl produced during MPO catalytic cycle can permeate through the PEG-coated nanotubes, resulting in the stripping of PEG and biodegradation.[43] However, MPO recognizes SWCNTs first, which is an electrostatically driven and selective process.[5] Once highly cationic MPO is placed in close proximity to ox-SWCNT (mostly present as SWCNT-COO^- under pH 7.4), oxidation of the nanotubes occurs in the vicinity of the bound enzyme. However, as the surface charge of DOX-SWCNT is different from that of ox-SWCNT due to the functionalization with PL-PEG and DOX, we further implemented zeta potential analysis to characterize the surface charge of each functionalization and find the effective concentration range of MPO that can bind with the drug conjugate (Fig. 4).

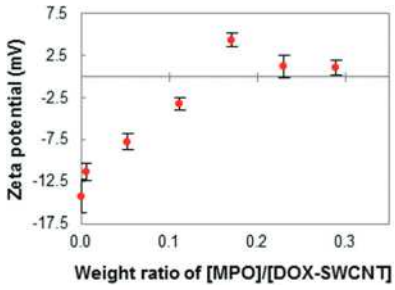

Fig. 4 Zeta potential titration of the DOX-SWCNT with MPO at pH 7.4. Data are means ± SD of five replicate measurements.

PL-PEG and DOX reduced the negative charge effect of ox-SWCNT in the synthesis of DOX-SWCNT, as indicated in the zeta potential change from −48.3 mV to −14.2 mV (see ESI, Table S1†), which could further delay the MPO-catalysed oxidation. To analyse the threshold binding ratio of MPO to DOX-SWCNT, we performed zeta potential titration by gradually adding MPO to a DOX-SWCNT solution. It appears that the binding of MPO became saturated near 0.18 weight equiv. We chose 0.13 weight equiv. (lower than the threshold value) for our degradation experiment, which probably resulted in the effective enzymatic oxidation with the drug conjugate. The fact that the addition of PL-PEG did not completely prevent the binding with MPO is interesting although, according to the literature,[47] some PEGs could reduce the non-specific interaction with MPO under certain circumstances.

To test whether cellular MPO- and peroxynitrite-dependent pathways may exhibit differential biodegradation activity towards free DOX and nanotube-bound DOX, we co-cultured fluorescent dye labeled B16 melanoma cells with each of the DOX samples in the presence of bone marrow-derived tumor-activated myeloid-derived suppressor cell (MDSC) known to express high levels of MPO and iNOS.[48] This implies that both MPO- and peroxynitrite-dependent oxidative biodegradation pathways are active in these cells. Importantly, both MPO and iNOS expression are essential for the immune-suppressive function of MDSC during growth of the tumor in the host.[49] Twenty-four hours later, DOX-induced apoptosis was assessed in B16 melanoma cells by Annexin V binding (as described in ESI†). Fig. 5a demonstrates the results of a representative flow cytometry analysis, and Fig. 5b shows the summary results from the triplicated experiments. As expected, free DOX in moderate pharmacological dose of 5 μM increased the level of tumor cell death up to two-fold ($p < 0.01$) whereas DOX-SWCNT was significantly more potent and caused an up to six-fold increase of apoptosis ($p < 0.01$). The concentrations of DOX released from the nanotubes in the cell medium remained constant (about 1 μM) over 24 h whereas free DOX concentrations were threefold higher than DOX-SWCNT initially and then dropped by about 50% after 24 h (Fig. S14†). However, direct comparison of cytotoxic effect of free DOX or nanotube-bound DOX is not appropriate in cell cultures due to the differences in concentrations and dynamics of DOX degradation. Important is the fact that the addition of MDSC significantly abolished the cytotoxic effect of free DOX, but not nanotube-bound DOX, suggesting that the nanotube-bound cytotoxic drug exhibits a stronger antitumor potential in the *in vitro* model of the tumor microenvironment than the free chemotherapeutic agent. As shown in Fig. 5, the absence of the cytotoxic effects in all additional control groups (ox-SWCNT/PL-PEG, MDSC alone, and MDSC+ox-SWCNT/PL-PEG) supports this conclusion.

The effects of free DOX and DOX-SWCNT on tumor cells in the presence of tumor-activated MDSC was confirmed using another tumor cell line – 3LL Lewis lung carcinoma, where tumor cell proliferation was determined. As shown in Fig. S16,† both free DOX and DOX-SWCNT decreased the

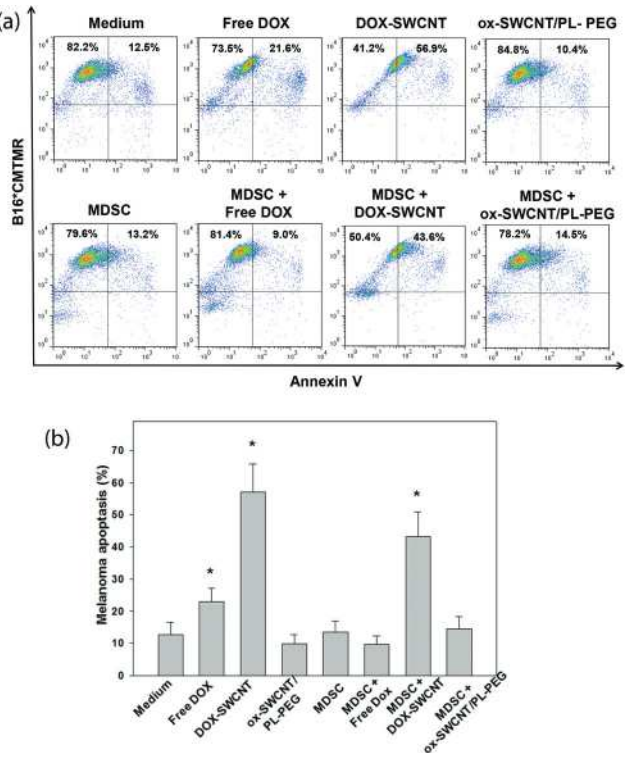

Fig. 5 Cytotoxic effects of free DOX *vs.* DOX-SWCNT in B16 melanoma cells and bone marrow-derived, tumor-activated MDSC. DOX-SWCNT, but not free DOX, induces significant apoptosis of B16 melanoma cells even in the presence of MDSC. B16 melanoma cells and bone marrow-derived tumour-activated MDSC were generated as described in ESI† and co-cultured in the presence of free DOX or DOX-SWCNT. ox-SWCNT/PL-PEG served as a control. The level of tumour cell apoptosis was determined 24 h later by Annexin V binding as described in ESI.† All cell cultures were set in triplicates, and results are shown as representative flow cytometry dot plots in (a) and the mean ± SEM (standard error of the mean) (N = 3) in (b). *, $p < 0.01$ *versus* control (medium) group (one way ANOVA).

number of 3LL cells in cultures up to two-fold ($p < 0.01$). However, addition of MDSC abolished the cytostatic/cytotoxic effect of free DOX, but not DOX-SWCNT, suggesting that nanotube-bound DOX exhibits a significantly stronger antitumor potential than free DOX in the presence of tumor-activated MDSC expressing high levels of MPO and iNOS.

Conclusions

We have demonstrated a degradable carbon nanotube-drug conjugate (DOX-SWCNT) by MPO-catalysed and peroxynitrite-mediated oxidations. The degradation behaviour of free DOX was analysed in comparison to DOX-SWCNT under the same conditions, which allowed us to evaluate the effect of the nanotube carrier on the stability of DOX towards the oxidative reactions by enzymatic systems of innate immune cells—particularly neutrophils and macrophages. In both of the oxidative conditions, the drug molecules (DOX-SWCNT) degraded more slowly than free DOX. Our *in vitro* study also suggests that the chemotherapeutic agent delivered by the nanocarrier may be protected from the enzymatic inactivation associated with myeloid cells in the tumor microenvironment while exhibiting a constant DOX release rate. However, DOX demonstrated pH-dependent degradation in the non-oxidative conditions, and the nanotube carrier seems to be ineffective in slowing down this degradation process. Optimizing the balance between the degradation and resistance of the drug carrier and the payload towards the oxidants generated by inflammatory cells is critical to meet the needs for safety and prolonged circulation while orchestrating the stability and therapeutic effect of the drug. This strategy opens opportunities for exploring new parameters in biodegradation and developing controllable degradation properties by chemical modification of the surface of nanotubes.

Acknowledgements

This work was supported by the National Institutes of Health, NIEHS R01ES019304, NCI RO1 CA154369, U19 AI068021, HL114453, and the National Institute for Occupational Safety and Health (NIOSH, OH008282). The authors thank Seth C. Burkert for performing X-ray photoelectron spectroscopy (XPS) analysis.

Notes and references

1 J. Shi, A. Votruba, O. Farokhzad and R. Langer, *Nano Lett.*, 2010, **10**, 3223–3230.
2 C. Fabbro, H. Ali-Boucetta, T. Da Ros, K. Kostarelos, A. Bianco and M. Prato, *Chem. Commun.*, 2012, **48**, 3911–3926.
3 F. Lian and B. Chen, *Curr. Med. Chem.*, 2010, **17**, 10–24.
4 K. Kostarelos, A. Bianco and M. Prato, *Nat. Nanotechnol.*, 2009, **4**, 627–633.
5 V. Kagan, N. Konduru, W. Feng, B. Allen, J. Conroy, Y. Volkov, I. Vlasova, N. Belikova, N. Yanamala, A. Kapralov, Y. Tyurina, J. Shi, E. Kisin, A. Murray, J. Franks, D. Stolz, P. Gou, J. Klein-Seetharaman, B. Fadeel, A. Star and A. Shvedova, *Nat. Nanotechnol.*, 2010, **5**, 354–359.
6 G. P. Kotchey, S. A. Hasan, A. A. Kapralov, S. H. Ha, K. Kim, A. A. Shvedova, V. E. Kagan and A. Star, *Acc. Chem. Res.*, 2012, **45**, 1770–1781.
7 A. Bianco, K. Kostarelos and M. Prato, *Chem. Commun.*, 2011, **47**, 10182–10188.
8 O. C. Farokhzad, J. Cheng, B. A. Teply, I. Sherifi, S. Jon, P. W. Kantoff, J. P. Richie and R. Langer, *Proc. Natl. Acad. Sci. U. S. A.*, 2006, **103**, 6315–6320.
9 T. M. Allen and P. R. Cullis, *Science*, 2004, **303**, 1818–1822.
10 A. Cartoni, P. Menna, E. Salvatorelli, D. Braghiroli, R. Giampietro, F. Animati, A. Urbani, P. Del Boccio and G. Minotti, *J. Biol. Chem.*, 2004, **279**, 5088–5099.
11 E. T. Morgan, *Drug Metab. Dispos.*, 2001, **29**, 207–212.

12 S. Reuter, S. C. Gupta, M. M. Chaturvedi and B. B. Aggarwal, *Free Radical Biol. Med.*, 2010, **49**, 1603–1616.
13 V. E. Kagan, A. A. Kapralov, C. M. St. Croix, S. C. Watkins, E. R. Kisin, G. P. Kotchey, K. Balasubramanian, I. I. Vlasova, J. Yu, K. Kim, W. Seo, R. K. Mallampalli, A. Star and A. A. Shvedova, *ACS Nano*, 2014, **8**, 5610–5621.
14 Z. Liu, A. Fan, K. Rakhra, S. Sherlock, A. Goodwin, X. Chen, Q. Yang, D. Felsher and H. Dai, *Angew. Chem., Int. Ed.*, 2009, **48**, 7668–7672.
15 Z. Liu, C. Davis, W. Cai, L. He, X. Chen and H. Dai, *Proc. Natl. Acad. Sci. U. S. A.*, 2008, **105**, 1410–1415.
16 Z. Ji, G. Lin, Q. Lu, L. Meng, X. Shen, L. Dong, C. Fu and X. J. Zhang, *Colloid Interface Sci.*, 2012, **365**, 143–149.
17 K. Welsher, Z. Liu, S. P. Sherlock, J. T. Robinson, Z. Chen, D. Daranciang and H. Dai, *Nat. Nanotechnol.*, 2009, **4**, 773–780.
18 G. Prencipe, S. M. Tabakman, K. Welsher, Z. Liu, A. P. Goodwin, L. Zhang, J. Henry and H. Dai, *J. Am. Chem. Soc.*, 2009, **131**, 4783–4787.
19 I. Hamad, O. Al-Hanbali, A. C. Hunter, K. J. Rutt, T. L. Andresen and S. M. Moghimi, *ACS Nano*, 2010, **4**, 6629–6638.
20 B. S. Zolnik, Á. Gonzalez-Fernández, N. Sadrieh and M. A. Dobrovolskaia, *Endocrinology*, 2010, **151**, 458–465.
21 R. M. Mainardes, M. P. D. Gremião, I. L. Brunetti, L. Marcos da Fonseca and N. M. Khali, *J. Pharm. Sci.*, 2009, **98**, 257–267.
22 P. L. Rodriguez, T. Harada, D. A. Christian, D. A. Pantano, R. K. Tsai and D. E. Discher, *Science*, 2013, **339**, 971–975.
23 M. B. Hampton, A. J. Kettle and C. C. Winterbourn, *Blood*, 1998, **92**, 3007–3017.
24 R. Radi, *J. Biol. Chem.*, 2013, **288**, 26464–26472.
25 J. Henderson and J. Heinecke, *Peroxidases and Catalases*, ed. H. B. Dunford, Wiley, Hoboken, NJ, 2010, ch. 16, pp. 257–269.
26 S. J. Klebanoff, *Leukocyte Biol.*, 2005, **77**, 598–625.
27 A. D. Gregory and A. M. Houghton, *Cancer Res.*, 2011, **71**, 2411–2416.
28 L. M. Coussens and Z. Werb, *Nature*, 2002, **420**, 860–867.
29 C. Szabó, H. Ischiropoulos and R. Radi, *Nat. Rev. Drug Discovery*, 2007, **6**, 662–680.
30 A. Denicola and R. Radi, *Toxicology*, 2005, **208**, 273–288.
31 J. P. Uetrecht, *Chem. Res. Toxicol.*, 1999, **12**, 387–395.
32 I. I. Vlasova, T. V. Vakhrusheva, A. V. Sokolov, V. A. Kostevich and A. A. Ragimov, *J. Phys.: Conf. Ser.*, 2011, **291**, 012056.
33 G. Kotchey, J. Gaugler, A. Kapralov, V. Kagan and A. Star, *J. Mater. Chem. B*, 2013, **1**, 302–309.
34 X. Liu, R. H. Hurt and A. B. Kane, *Carbon*, 2010, **48**, 1961–1969.
35 Y. Zhao, B. L. Allen and A. Star, *J. Phys. Chem. A*, 2011, **115**, 9536–9544.
36 G. Kotchey, Y. Zhao, V. E. Kagan and A. Star, *Adv. Drug Delivery Rev.*, 2013, **65**, 1921–1932.
37 K. Flavin, I. Kopf, E. Del Canto, C. Navio, C. Bittencourt and S. Giordani, *J. Mater. Chem.*, 2011, **21**, 17881–17887.
38 S. Ghosh, S. M. Bachilo and R. B. Weisman, *Nat. Nanotechnol.*, 2010, **5**, 443–450.
39 H. Huang, Q. Yuan, J. S. Shah and R. D. K. Misra, *Adv. Drug Delivery Rev.*, 2011, **63**, 1332–1339.
40 Z. Liu, X. M. Sun, N. Nakayama-Ratchford and H. Dai, *ACS Nano*, 2007, **1**, 50–56.
41 J. Hurst, *Peroxidase in Chemistry and Biology*, ed. J. Everse, K. E. Everse and M. B. Grisham, CRC press, Boca Raton, Fl, 2000, vol. 1, pp. 37–62.
42 I. I. Vlasova, T. V. Vakhrusheva, A. V. Sokolov, V. A. Kostevich, A. A. Gusev, S. A. Gusev, V. I. Melnikova and A. S. Lobach, *Toxicol. Appl. Pharmacol.*, 2012, **264**, 131–142.
43 K. Bhattacharya, C. Sacchetti, R. El-Sayed, A. Fornara, G. P. Kotchey, J. A. Gaugler, A. Star, M. Bottini and B. Fadeel, *Nanoscale*, 2014, **6**, 14686–14690.
44 H. B. Dunford, *Peroxidases and Catalases*, ed. H. B. Dunford, Wiley, Hoboken, NJ, 2010, ch. 3, pp. 13–39.
45 G. Powis, *Free Radical Biol. Med.*, 1989, **6**, 63–101.
46 J. H. Beijnen, O. A. J. G. Van der Houwen and W. J. M. Underberg, *Int. J. Pharm.*, 1986, **32**, 123–131.
47 D. E. Owens III and N. A. Peppas, *Int. J. Pharm.*, 2006, **307**, 93–102.
48 Y. Zhao, S. C. Burkert, Y. Tang, D. C. Sorescu, A. A. Kapralov, G. V. Shurin, M. R. Shurin, V. E. Kagan and A. Star, *J. Am. Chem. Soc.*, 2015, **137**, 675–684.
49 S. Solito, L. Pinton, V. Damuzzo and S. Mandruzzato, *Immunol. Invest.*, 2012, **41**, 722–737.

